Sensors & Actuators: B. Chemical 444 (2025) 138510

Contents lists available at ScienceDirect

Sensors and Actuators: B. Chemical

journal homepage: www.elsevier.com/locate/snb

HOF-on-MOF heterostructured enzyme mimic with high catalytic activity for colorimetric detection of β-bungarotoxin

Xiang Lai [a,1], Xiaoqin Deng [a,1], Tan Feng [a,1], Lishen Yang [a], Xingye Zheng [a], Hang Chen [a], Fengqi Zhou [a], Hongmin Zhu [a], Jing Zeng [b], Wen-Hui Lee [c], Hui Zhao [d,*], Can-Peng Li [a,*]

[a] Bio-X Center for Interdisciplinary Innovation, School of Chemical Science and Technology, Yunnan University, Kunming 650091, PR China
[b] School of Materials and Energy, Yunnan University, Kunming 650091, PR China
[c] Key Laboratory of Animal Models and Human Disease Mechanisms of the Chinese Academy of Sciences/Key Laboratory of Bioactive Peptides of Yunnan Province, Kunming Institute of Zoology, The Chinese Academy of Sciences, Kunming, Yunnan, PR China
[d] Laboratory for Conservation and Utilization of Bio-resource, Yunnan University, Kunming 650091, PR China

ARTICLE INFO

Keywords:
HOF-on-MOF
Peroxidase-like activity
Laccase-like activity
Colorimetric detection
β-bungarotoxin

ABSTRACT

Snakebite envenomation represents a significant global emergency health concern, necessitating rapid and accurate medical intervention. Accurate detection and identification of snake venom are essential not only for clinical diagnosis but also for ecological conservation efforts. In this study, we report the synthesis of a hydrogen-bonded organic framework-on-metal-organic framework (HOF-on-MOF) heterostructured material, engineered through the synergistic interactions of robust hydrogen bonds and π-π stacking forces. This material demonstrates unique dual enzyme-mimetic properties, exhibiting both highly peroxidase-like and laccase-like catalytic activities. By utilizing the carboxyl groups on the surface of HOF-on-MOF, we developed a biosensor (HOF-on-MOF-β-BGT-apt) using an amino-modified β-bungarotoxin aptamer (NH_2-β-BGT-apt) via amide bonding. Combining the dual enzyme-mimetic activity of the HOF-on-MOF composite material, we designed a colorimetric biosensor capable of dual-signal detection of β-bungarotoxin (β-BGT), enabling sensitive and intuitive detection with a low detection limit. The applicability of the colorimetric sensor for β-BGT detection in human serum was assessed, highlighting its significant potential for biosensing and clinical diagnosis.

1. Introduction

Snakebite envenomation is a tropical disease that needs attention, but its associated dangers are often underestimated. Snakebites can result in varying degrees of toxicity, encompassing mild localized symptoms to severe systemic manifestations [1]. According to the World Health Organization (WHO), the global annual death toll from snake bites exceeds 80,000, with the highest incidence observed in South Asia [2]. Moreover, snakebite poses a significant challenge in numerous regions with insufficient medical resources, leading to ineffective treatment and underreporting of numerous cases [3]. Snake venom composition varies across species, yet its core components—proteins, peptides, enzymes, and small molecules—consistently drive envenomation pathogenesis [4]. Proteins and peptides constitute the principal constituents of snake venom, eliciting robust biological responses. These responses encompass neurotoxicity, resulting in the paralysis of the central nervous system; cytotoxicity, resulting in cellular destruction; and hemotoxicity, compromising blood clotting and inducing tissue damage [5]. These toxins initiate a cascade of immune reactions within the victim's body, contributing to the severity of the envenomation [2]. However, due to the high metabolic cost associated with venom production, it is possible for a venomous snake to deliver a dry bite, without injecting venom, when biting a victim [6]. Dry bites may occur in any snakebite incident, complicating clinical differentiation between envenomation and non-envenomation due to overlapping local symptoms (e.g., inflammation). Therefore, timely detection of toxins is significant for snakebite treatment. Snake venom detection offers a rapid and precise approach to ascertain whether a victim has been envenomated, aiding medical professionals in selecting appropriate treatment strategies. Recently, researchers have developed several reliable methods for snake venom detection [7–9].

Among them, the enzyme-linked immunosorbent assay (ELISA) has

* Corresponding authors.
E-mail addresses: zhaohui@ynu.edu.cn (H. Zhao), lcppp1974@sina.com (C.-P. Li).
[1] These authors contributed equally to this work

https://doi.org/10.1016/j.snb.2025.138510
Received 5 March 2025; Received in revised form 26 July 2025; Accepted 9 August 2025
Available online 11 August 2025

emerged as an ideal detection method, following numerous improvements. It is capable of meeting the requirements for detecting nanogram quantities of snake venom in the environment [8]. Nong et al. developed specific antibodies and created a sandwich ELISA, which demonstrated exceptional sensitivity and ultra-low detection limits for *Bungarus multicinctus* venom [10]. Similarly, Lee et al. utilized immunoglobulin G (IgG) and horseradish peroxidase (HRP) in a sandwich ELISA setup to diagnose snakebites, offering a viable immunological approach for venom detection [11]. However, traditional ELISA methods, which rely on natural enzymes like HRP, face several limitations, including challenges in enzyme preparation, storage, and susceptibility to inactivation [12,13]. Moreover, the covalent binding of enzyme-antibody conjugates in conventional setups can reduce the assay's sensitivity [14]. The advent of nano-enzymes has provided a solution to these issues, with researchers exploring their superior physicochemical properties as promising substitutes for natural enzymes. Additionally, the integration of nanomaterials and biosensors has led to the development of detection methods that are not only more sensitive but also faster. For instance, Lv et al. introduced Fe-N-C single-atom nano-enzymes (Fe-N_x SANs), which replaced traditional enzymes in ELISA kits, significantly improving the sensitivity of amyloid beta 1–40 detection [15]. Despite their effectiveness, the complex covalent interactions between antibodies and nanomaterials remain a critical factor in maintaining the accuracy and reliability of these assays [14].

In recent years, metal-organic frameworks (MOFs) and hydrogen-bonded organic frameworks (HOFs) have attracted much attention due to their unique physicochemical properties. HOFs are a class of porous organic materials self-assembled by hydrogen bonding, which are widely used in science and industry with the advantages of high tunability, large specific surface area, selective adsorption and environmental friendliness [16–18]. Their mild preparation process and good compatibility with enzymes make them ideal platforms for enzyme immobilization and can effectively retain enzyme activity [19,20]. In contrast, MOFs are materials known for their outstanding stability and abundant catalytic sites, making them promising candidates for various applications [21]. Although HOFs and MOFs each exhibit distinct strengths, their functionalities are inherently complementary in specific contexts, such as structure and stability [22], proton conduction mechanism [22–24], and functionalized integration [25,26]. The MOF surface was chemically modified by introducing functional groups capable of forming hydrogen bonds with HOF monomers, which promoted the growth of HOF on the MOF surface to form a layered structure with regular pores, and finally generated HOF-on-MOF composites [27]. By combining HOF and MOF, Li et al. developed a novel hybrid entangled frame structure, which not only improves the structural stability, but also significantly enhances the proton conduction properties [22]. Ma et al. reported a MOF@HOF core-shell material with higher photocatalytic efficiency and stability compared to single MOF or HOF [23]. The combination of HOF and MOF materials is a very promising area of research. In the field of sensing, this hybrid material offers high sensitivity and selectivity, high stability and biocompatibility, providing new ideas for the development of high-performance sensors [28–30].

The *Bungarus multicinctus,* regarded as the most venomous snake in Asia, owes its distinction to a remarkably high mortality rate. Among its toxic components, β-BGT primarily targets the nervous system, with a pronounced effect on the neuromuscular junction [31,32]. In this study, we constructed a bioprobe using HOF-on-MOF and NH_2-β-BGT-apt for the detection of β-BGT by ELISA, as shown in Scheme 1. The HOF-on-MOF was obtained by assembling the Cu-MOF and the HOF through hydrogen bonding and π-π interaction forces. The enzyme-like activities of Cu-MOF and HOF-on-MOF were compared by catalyzing characteristic chromogenic reactions with different groups of substrates, such as [TMB+H_2O_2] and [2,4-DP+ 4-AP]. Based on the excellent dual-enzyme-like activity of HOF-on-MOF, a dual-signal colorimetric method was developed to detect β-BGT of *Bungarus multicinctus*. In this study, we developed a dual-signal colorimetric assay based on HOF-on-MOF composites, which overcame the dependence of traditional ELISA on natural enzymes by integrating the enzyme compatibility of HOF with the catalytic activity of MOF, and enhanced the sensitivity and stability of β-BGT detection. Research and application of venom detection in venomous snakes provide crucial scientific evidence for the treatment of snakebites.

2. Experimental section

2.1. Synthesis of HOF-on-MOF

Cu-MOF (20 mg) and 1,3,6,8-tetrakis (*p*-benzoic acid) pyrene (H_4TBAPy) (5 mg) were dispersed in 40 mL of DMF. The mixture was first stirred at room temperature for 12 h, followed by heating at 120℃

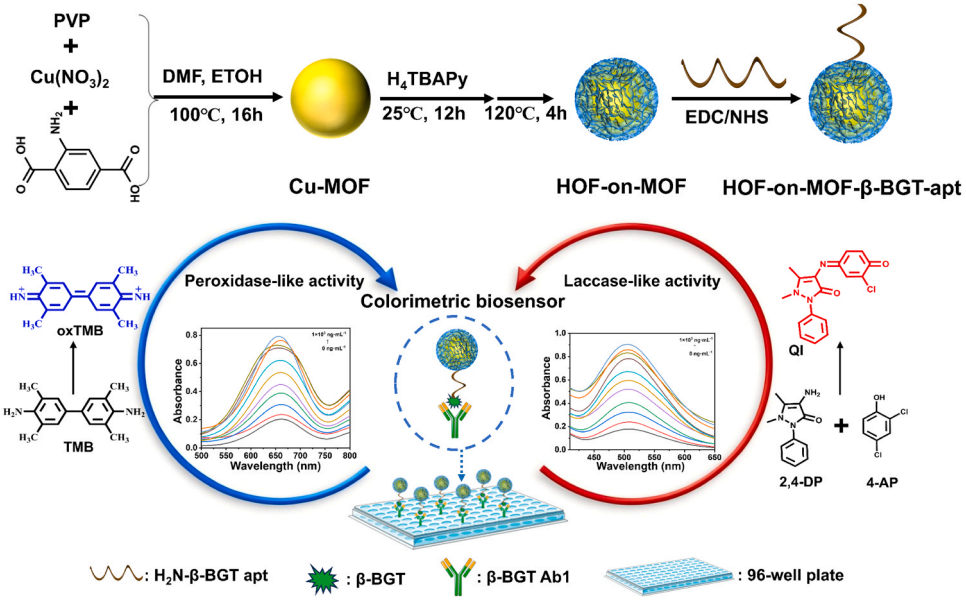

Scheme 1. Schematic illustration of preparation of hydrogen-bonded organic framework-on-metal-organic framework heterostructured enzyme mimic for detection of β-BGT.

for 4 h. After the mixture cooled down, stirring was maintained and the mixture was supplemented with 10 mL of water as well as 5 mg of H_4TBAPy. The composite material HOF-on-MOF was obtained by centrifugation and drying.

2.2. Preparation of biological probes

Firstly, HOF-on-MOF (1 mg) was dispersed in 1 mL of PBS, then EDC/NHS (EDC/NHS, 1/1) mixture (100 μL, 0.1 M) was added and stirred at room temperature for 2 h. Then 100 μL of NH_2-β-BGT-apt (2 μM) was added, and the stirring was continued for 12 h. The mixture was centrifuged at 8 000 rpm for 15 min and washed three times with PBS solution at pH 7.2 to obtain HOF-on-MOF-β-BGT-apt bioprobe.

2.3. Mechanism detection

Firstly, terephthalic acid (TA) was used as a probe to study hydroxyl radicals (•OH) in the reaction system. 700 μL of HAc-NaAc (0.01 M, pH 4.0) solution, 100 μL of H_2O_2 (10 mM), 100 μL of TA (5 mM) and 100 μL of HOF-on-MOF (200 μg mL^{-1}) were mixed and incubated at 25℃ for 6 h. The fluorescence of the mixed solution was measured at an excitation wavelength of 315 nm.

Secondly, •OH and superoxide anions ($O_2^{\bullet-}$) were further studied by electron paramagnetic resonance (EPR) using 5,5-dimethyl-1-pyrroline N-oxide (DMPO) as the trapping agent. In short, 790 μL of HAc-NaAc (0.01 M, pH 4.0) solution, 100 μL of H_2O_2 (10 mM), 10 μL of DMPO and 100 μL of HOF-on-MOF (200 μg mL^{-1}) and incubated at 25℃ for 5 min. The EPR was measured in capillary tubes.

Thirdly, we utilized 9,10-diphenylanthracene (DPA) to investigate singlet oxygen ($^1O_2$) in the reaction system. Initially, 0.5 mg of DPA was introduced to a 10 mL acetonitrile solution, the resulting mixture underwent oxygenation in a dark environment for 30 min. Subsequently, 1 mL of HOF-on-MOF (1 mg mL^{-1}) was added. The solution was then irradiated with a UV lamp at a wavelength of 365 nm. The absorbance of DPA at 355 nm was recorded using a UV spectrophotometer. Additionally, 2,2,6,6-tetramethylpiperidine (TEMP) served as a free radical scavenger, and $^1O_2$ production was confirmed through electron paramagnetic resonance (EPR) [33].

2.4. Colorimetric detection of β-BGT

The peroxide-like activity of HOF-on-MOF was evaluated by detecting β-BGT using the following protocol: (1) 100 μL of β-BGT primary antibody at a concentration of 2 μg mL^{-1} was added to 96-well plates and incubated at 4℃ overnight. (2) The plate was then washed three times with PBST (PBS containing 0.1 % Tween 20) and blocked with a 1 % BSA solution for 60 min at room temperature, followed by another wash with PBST. (3) The β-BGT solution with a concentration of 0.0001–1000 ng mL^{-1} was added to the treated 96-well plate, incubated at room temperature for 60 min, and cleaned the 96-well plate with PBST for three times. (4) Next, 100 μL of HOF-on-MOF-β-BGT-apt bioprobe was added dropwise to the plate, followed by incubation at room temperature for 60 min and three washes with PBST. (5) Finally, 150 μL of TMB (10 mM) and 150 μL of HAc-NaAc (pH=4.5) solution were added to the 96-well plate and incubated at 37℃ for 30 min. The absorbance of the reaction system was recorded using an enzyme-labeler.

For HOF-on-MOF with laccase-like activity, 75 μL of 4-AP (1 mg mL^{-1}), 75 μL of 2,4-DP (1 mg mL^{-1}) and 100 μL of MES (pH=6.8) solution were added to step (5) and incubated at 65℃ for 30 min. The absorbance of the reaction system was recorded using the same enzyme-labeled apparatus.

3. Results and discussion

3.1. Characterization of HOF-on-MOF

The synthesis of HOF-on-MOF with enzyme-like activity aimed to achieve the combination of HOF and Cu-MOF in the solvent DMF. Fourier transform infrared (FTIR) spectroscopy confirmed the functional group structures of HOF, Cu-MOF and HOF-on-MOF (Fig. 1**A**). For HOF, the peak at 1692 cm^{-1} was classified as a stretching vibration of -C═O. For Cu-MOF, the peak at 3377 cm^{-1} was attributed to the amine group's asymmetric and symmetric stretching vibrations, confirming the presence of amino groups in the structure. The stretching vibration peak of -OH at 2970 cm^{-1} disappears, confirming the occurrence of coordination interaction between Cu^{2+} and −COOH of organic ligand [34] (Fig. S1). For HOF-on-MOF, the characteristic peak intensity at 1692 and 3377 cm^{-1} were lower than those of HOF and Cu-MOF, indicating a coordination interaction between the -COOH of the H_4TBAPy monomer and the -NH_2 of Cu-MOF. In addition, the characteristic peaks at 1564 and 1607 cm^{-1} were attributed to HOF and HOF-on-MOF Skeleton vibration of pyrene rings in structures. The X-ray diffraction (XRD) patterns of HOF and HOF-on-MOF (Fig. 1**B**) exhibited diffraction peaks at 2θ= 4.7°, which was consistent with the literature results [35] and confirmed the successful preparation of the materials. Moreover, the zeta potential of HOF, Cu-MOF and HOF-on-MOF was −24.8 mV, −9.78 mV and −14.9 mV, respectively (Fig. S2).

The X-ray photoelectron spectroscopy (XPS) spectra of HOF-on-MOF were further recorded with the aim of analyzing the elemental compositions and chemical states. As shown in Fig. 1**C**, the presence of C, N, O and Cu elements was observed in both Cu-MOF and HOF-on-MOF. The Cu 2p spectra in Fig. 1**D** exhibit two characteristic peaks, namely Cu $2p_{1/2}$ (954.5 eV) and Cu $2p_{3/2}$ (934.7 eV), representing distinct chemical states of copper. The binding energies of 933.5 and 952.8 eV represent characteristic peaks of Cu^+[36], while the binding energies of 934.9 and 954.7 eV were characteristic peaks of Cu^{2+}[37]. This suggests the presence of oxidation-reduction ion pairs in the multifunctional catalytic system. In addition, the peaks at 939.8, 943.9, and 962.5 eV were attributed to the satellite peaks, which may arise from the presence of $3d^9$ orbitals of Cu^{2+} ions.

The microscopic morphologies of Cu-MOF and HOF-on-MOF were further observed. As shown in Fig. 2**A-D**, Cu-MOF showed a uniformly distributed spherical structure, with an average particle size of approximately 487 nm. In contrast, HOF-on-MOF showed a distinct core-shell HOF-on-MOF structure. The microscopic morphology of the HOF-on-MOF material boundary was observed by TEM in Fig. S3. In the HOF-on-MOF structure, the spherical Cu-MOF serves as the core, enveloped by a lamellar HOF layer, reinforcing the core-shell configuration. Elemental mapping revealed the presence of C, N, O, and Cu element in HOF-on-MOF, with C and O predominating in the shell layer, as illustrated in Fig. 2**E**. This composition suggests that the inner core is composed of Cu-MOF, while the outer shell consists of a lamellar HOF structure developed on the Cu-MOF surface, culminating in a core-shell architecture. Such a unique structure boasts a vast specific surface area and superior substrate binding sites, enhancing its efficiency in catalytic reactions.

3.2. Peroxidase-like activity and catalytic kinetics of HOF-on-MOF

To study the peroxidase-like activity of Cu-MOF and HOF-on-MOF, TMB was used as the enzyme-like substrate. In Fig. 3**B**, the addition of Cu-MOF or HOF-on-MOF into the [TMB+H_2O_2] solution resulted in a color change from colorless to dark blue, confirming the peroxidase-like activity of both materials. Notably, the peroxidase-like activity of HOF-on-MOF was significantly enhanced following the complexation process compared to that of Cu-MOF alone, potentially due to the larger specific surface area and higher substrate affinity of HOF. Further examination (Fig. S4) revealed that the optimal temperature for this peroxidase-like

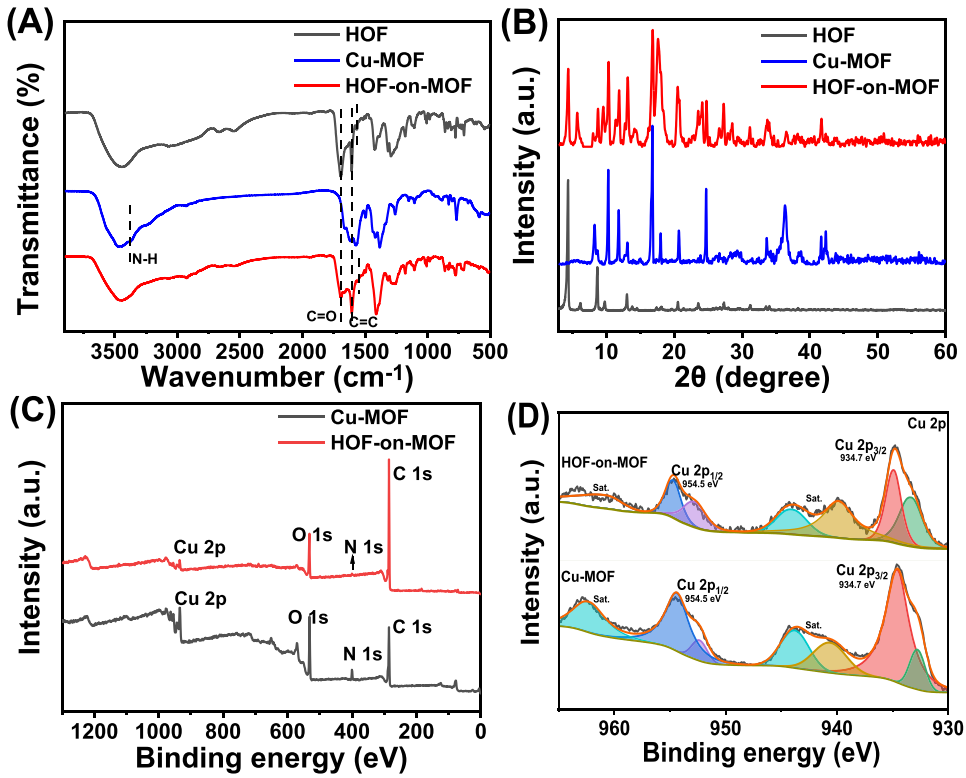

Fig. 1. (A) FTIR and (B) XRD spectra of HOF, Cu-MOF and HOF-on-MOF; XPS spectra of Cu-MOF and HOF-on-MOF: (C) survey, and (D) high-resolution Cu 2p spectra.

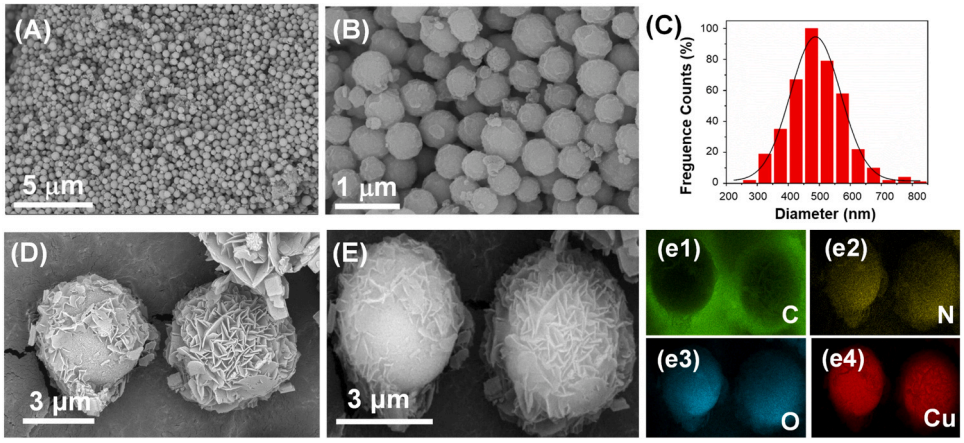

Fig. 2. (A, B) SEM image of Cu-MOF; (C) Average size distribution of Cu-MOF; (D) SEM image of HOF-on-MOF; (E) EDS elemental mapping of HOF-on-MOF.

activity of HOF-on-MOF was 37°C, with an optimum pH of 4.0.

The Michaelis-Menten kinetic determined the catalytic kinetic parameters of Cu-MOF and HOF-on-MOF. As shown in Fig. 3**C, 3D** and Fig. S5, the catalysis of TMB follows typical Michaelis-Menten behavior. The K_m of Cu-MOF and HOF-on-MOF were calculated to be 0.097 mM and 0.045 mM in Table 1, respectively.

3.3. Laccase-like activity of HOF-on-MOF

To investigate the laccase-like activity of Cu-MOF and HOF-on-MOF, 2,4-DP and 4-AP serve as substrates. As shown in Fig. 4**B**, the initial solution remained colorless in the presence of 2,4-DP and 4-AP. Upon addition of Cu-MOF or HOF-on-MOF, a red color developed, accompanied by characteristic absorption at 510 nm, confirming the laccase-like activity of both materials. Interestingly, HOF-on-MOF exhibited a deeper coloration compared to Cu-MOF alone, suggesting an enhanced laccase-like activity in the composite material. Furthermore, the optimum conditions for HOF-on-MOF as a laccase-like catalytic substrate were investigated. As shown in Fig. S6, the maximum activity was observed at 65°C, with an optimum pH of 6.5.

To investigate the kinetic performance of the laccase-like activity of Cu-MOF and HOF-on-MOF, 2,4-DP was utilized as the reaction substrate. The absorbance of the reaction system was recorded at 510 nm, and the reaction rate obtained was shown in Fig. 4**C, D** and Fig. S7. The Michaelis-Menten reaction parameters were presented in Table 2, revealing that the K_m value for HOF-on-MOF was 0.038 mM, markedly lower than that of Cu-MOF. This significant difference indicates the strong substrate affinity of HOF-on-MOF for 2,4-DP. The catalytic mechanism of natural laccase has been studied by Solomon et al. [42]. The potential laccase-like activity mechanism of HOF-on-MOF can be

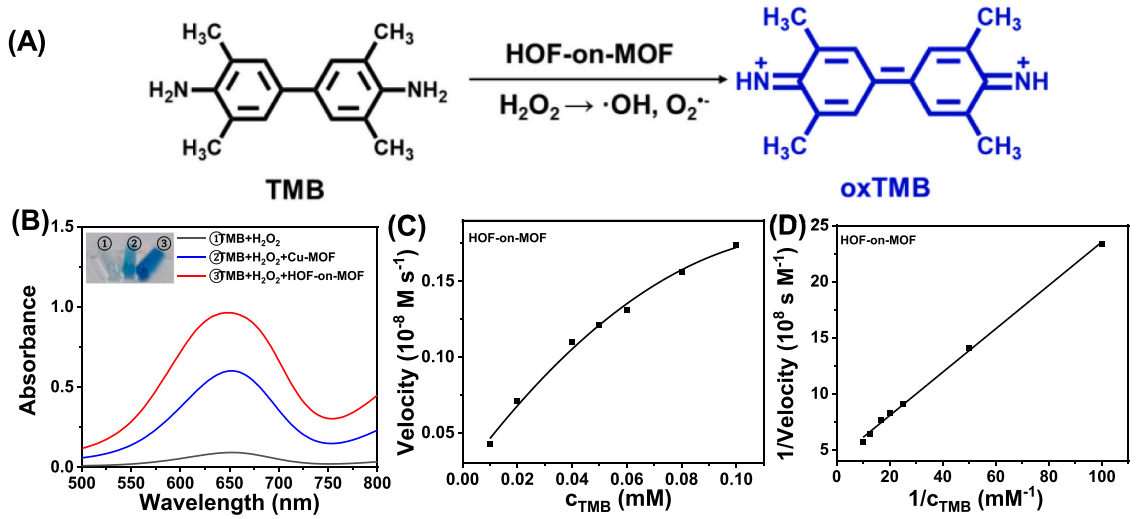

Fig. 3. (A) Oxidation reaction from TMB to oxTMB catalyzed by HOF-on-MOF in the presence of H_2O_2. (B) UV–vis spectra of different reaction groups. Steady-state kinetic assays of HOF-on-MOF. (C) Michaelis-Menten curves for different concentrations of TMB, and (D) Corresponding Lineweaver-Burk diagram.

Table 1
Comparison of catalyst kinetic parameters of HOF-on-MOF and other materials or nature enzyme HRP.

Materials	Substrate	K_m (mM)	V_{max} ($\times 10^{-8}$ Ms^{-1})	Ref.
HRP	TMB	0.434	3.7	[38]
Cu-MOF	TMB	2.55	21.47	[39]
Cu-BDC@$FeMo_6$	TMB	0.45	0.16	[40]
Cu FMA	TMB	1.1	1.79	[41]
Cu-MOF	TMB	0.097	29	this work
HOF-on-MOF	TMB	0.045	24	this work

inferred, as shown in Fig. 4**E**. The potential mechanism of laccase-like activity of HOF-on-MOF consists of four steps, namely substrate binding, substrate oxidation, electron transfer and O_2 reduction [43,44]. Briefly, due to Cu^{I} having a higher oxidation ability than Cu^{II}, phenol substrate 2,4-DP is oxidized by Cu^{I}. To verify the essential role of oxygen in the laccase-catalyzed oxidation process, nitrogen (N_2) was introduced into the reaction system, and changes in the solution's absorption spectra were monitored (Fig. S8). The absorbance of the samples in the presence of air was consistently higher than that observed under N_2 conditions, suggesting that the catalytic activity of laccase is strongly dependent on the availability of dissolved oxygen.

3.4. Catalytic mechanism

Peroxidase-like catalytic mechanisms are broadly categorized into two pathways: the generation of reactive oxygen species (ROS), such as •OH, and electron transfer processes occurring during the reaction. To investigate the catalytic mechanism of HOF-on-MOF composites, TA was employed as a fluorescent probe to detect and confirm the generation of •OH radicals within the system.

Further, to capture possible ROS during catalysis using EPR, DMPO reagent was selected as •OH/$O_2^{\bullet-}$ trapping agent, and TEMP was used to capture $^1O_2$. In the EPR characteristic spectrum of •OH in Fig. 5**B**, the [H_2O_2+HOF] group appears as a straight line, indicating the inability of HOF to generate •OH. In contrast, both the [H_2O_2+Cu-MOF] and [H_2O_2+HOF-on-MOF] groups exhibit typical quadruple peaks of •OH, providing evidence that both Cu-MOF and HOF-on-MOF are capable of producing •OH. Similarly, EPR was used to confirm the presence of $O_2^{\bullet-}$ and the result was shown in Fig. 5**C**. Both Cu-MOF and HOF-on-MOF exhibited a sixfold characteristic peak for $O_2^{\bullet-}$, indicating that they both can produce $O_2^{\bullet-}$, while HOF did not exhibit such characteristics.

To test $^1O_2$, 9, 10-diphenyl (DPA) was used as a $^1O_2$ scavenger. As shown in Fig. S9B, the [DAP+Cu-MOF] group showed little change in UV–vis absorption at 355 nm, indicating the inability of Cu-MOF to generate $^1O_2$. Conversely, significant decreases in UV–vis absorption spectra at 355 nm were observed after the addition of HOF and HOF-on-MOF, as shown in Fig S9C and S9D, suggesting their capability to produce $^1O_2$. The generation of $^1O_2$ was further verified using EPR, as shown in Fig. 5**D**. The addition of Cu-MOF did not yield the characteristic triple peak of $^1O_2$, indicating its incapacity to produce $^1O_2$. In contrast, both HOF and HOF-on-MOF exhibited characteristic peaks of $^1O_2$ in the EPR spectra.

Based on the above results, the mechanism of Cu-MOF and HOF-on-MOF is attributed to the formation of •OH and $O_2^{\bullet-}$ in the reaction system. HOF-on-MOF produced more free radicals than Cu-MOF, which was mainly attributed to the promotion of proton migration by its porous structure, the stability of HOF, and the synergistic effect of the two synergistic actions [22]. In addition, the introduction of hydrogen bonding sites helps to promote the proton-coupled electron transfer (PCET) process, which accelerates the rate of electron transfer between it and molecular oxygen and improves the catalytic activity [47].

3.5. Detection of β-BGT

β-BGT is a presynaptic polypeptide neurotoxin predominantly present in the venom of *Bungarus multicinctus*, where it constitutes the primary active component. Upon exposure to the toxin, the body can experience neurological impairments, which, if not promptly treated, may lead to fatal outcomes [48]. Therefore, it is imperative to establish a reliable and sensitive method for the detection of β-BGT in practical applications. The performance of the developed ELISA was assessed using a UV–visible spectrophotometer at 652 nm, where the absorbance values increased in direct proportion to the concentration of β-BGT, demonstrating the assay's sensitivity (Fig. 6**A**). Fig. 6**B** showed a linear relationship between the absorbance values and logarithm of β-BGT concentrations in the range from 0.0001–1000 ng·mL^{-1}, expressed as $A = 0.078 \log C_{\beta\text{-BGT}} + 0.5348$ ($R^2 = 0.9982$), and the LOD was 2.9×10^{-5} ng·mL^{-1}. Furthermore, the laccase-like activity of HOF-on-MOF can be utilized for detecting different concentrations of β-BGT at 510 nm. Fig. 6**C** showed the absorbance change at 510 nm wavelength proportional to the β-BGT concentration. In Fig. 6**D**, the absorbance of the reaction system has a linear relationship with the logarithm of β-BGT concentration, represented by the equation $A = 0.0941 \log C_{\beta\text{-BGT}} + 0.6013$ ($R^2 = 0.9984$), with a LOD of 5.15×10^{-6} ng·mL^{-1}.

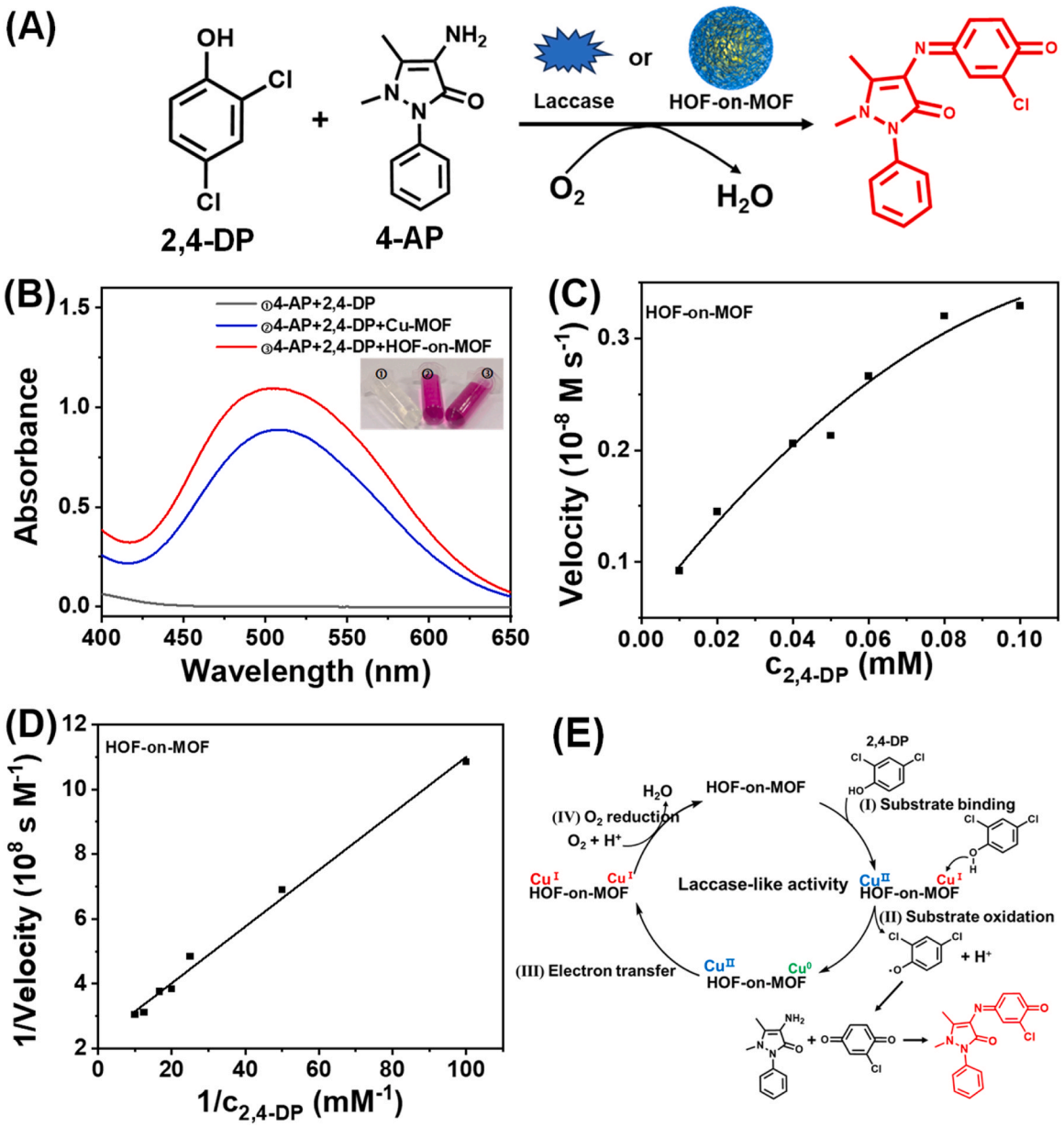

Fig. 4. (A) Schematic representation of the color development reaction catalyzed by laccase or HOF-on-MOF, (B) UV–vis spectra of different reaction groups. Steady-state kinetic assays of HOF-on-MOF: (C) Michaelis-Menten curves for different concentrations of 2,4-DP, and (D) Corresponding Lineweaver-Burk diagram. (E) Potential mechanism of laccase-like activity of HOF-on-MOF.

Table 2
Comparison of other catalyst kinetic parameters.

Materials	Substrate	K_m (mM)	V_{max} ($\times 10^{-8}$ Ms^{-1})	Ref.
Laccase	2,4-DP	0.41	10.68	[45]
CH-Cu	2,4-DP	0.42	12.2	[45]
Cu FMA	2,4-DP	0.45	5.72	[41]
Bpy-Cu	2,4-DP	0.19	2.47	[46]
Cu-MOF	2,4-DP	0.091	0.45	this work
HOF-on-MOF	2,4-DP	0.038	0.43	this work

Additionally, the linear detection range and LOD of this method were compared with those of existing snake venom detection techniques, as shown in Table S1. The established method exhibits a wide linear detection range and a low LOD, underscoring its strong potential for detecting β-BGT in *Bungarus multicinctus* venom.

3.6. Repeatability, stability, and anti-interference of biosensor

The peroxidase-like activity of the bioprobe was employed to evaluate its repeatability, stability, and resistance to interference. Repeatability tests, shown in Fig. S10A, demonstrated consistent results, confirming the method's reproducibility. Storage stability tests, depicted in Fig. S10B, indicated that the bioprobe maintained over 98 % of its enzyme activity after one month of storage. Furthermore, interference experiments with biological probes, illustrated in Fig. S10C, revealed that the colorimetric biosensor constructed using this method exhibited minimal interference from common venomous snake toxins. These findings underscore the excellent specificity of the bioprobe-based colorimetric biosensor.

3.7. Real sample analysis

The recovery rate of β-BGT was assessed by spiking human serum

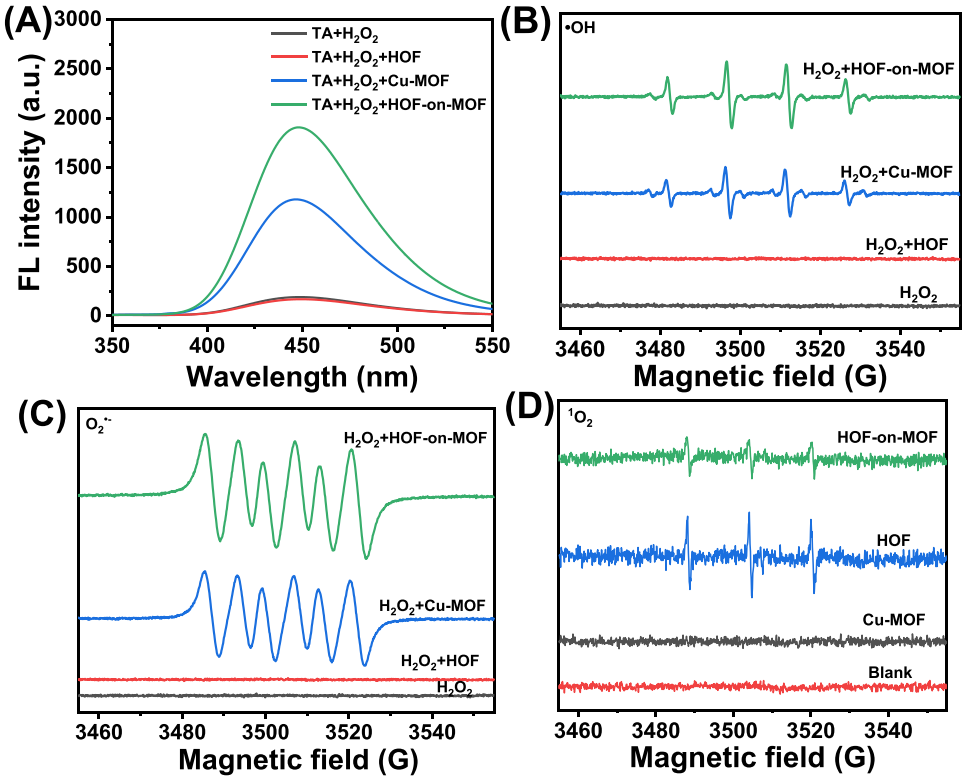

Fig. 5. (A) TA was used as a fluorescent probe to study the effect of •OH formation. The EPR spectra of (B) •OH, (C) $O_2^{\bullet-}$ and (D) $^1O_2$ were determined.

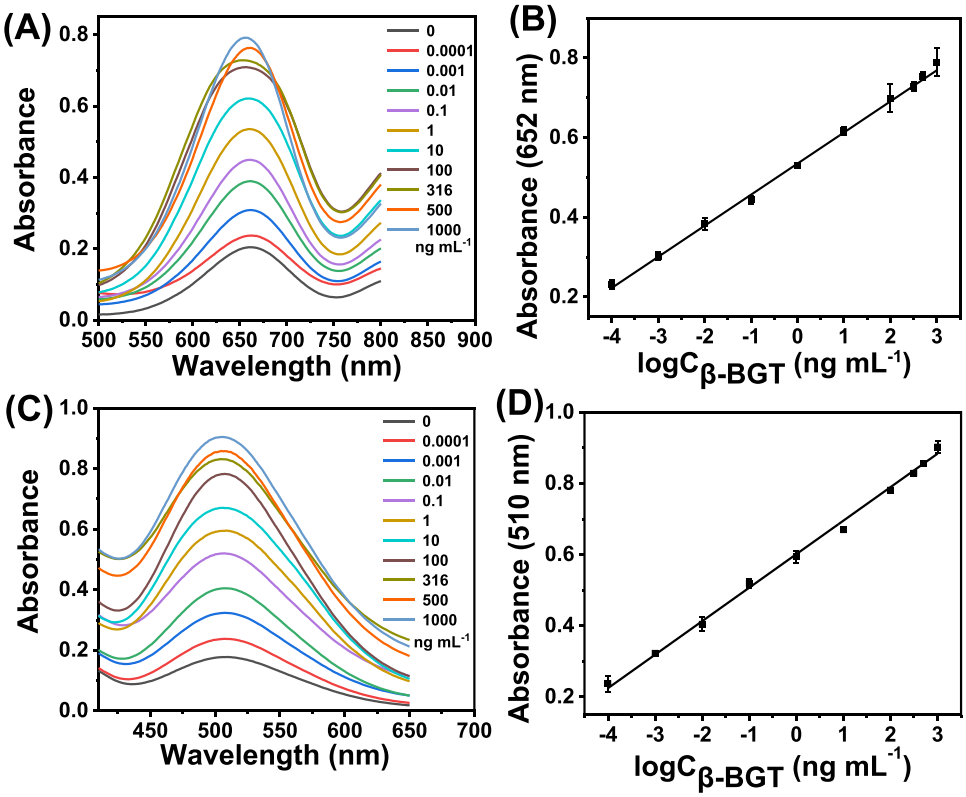

Fig. 6. Detection of β-BGT by HOF-on-MOF: (A) UV–vis absorption curves and (B) linear relationships based on peroxidase-like activity methods; (C) UV–vis absorption curves and (D) linear relationships based on laccase-like activity methods. Data represents the mean±standard deviation (n = 3).

samples with a known concentration of β-BGT standard. The results, presented in Table S2, showed recovery rates ranging from 95.88 % to 106.40 %, with standard deviations of 2.38–3.31 %. These results confirm that the established method is effective for detecting β-BGT in real-world samples, ensuring reliable recovery rates.

To validate the practical applicability of the developed sensor in real-world sample detection, we carried out experiments using tissue fluid samples containing *Bungarus multicinctus* snake venom. Fig. S11 showed the results of the 30 samples tested, including 26 positive samples and 4 negative samples detected. Among them, 26 samples tested positive. The sensor exhibited a high level of accuracy in identifying positive cases, though two negative samples yielded false-positive readings.

4. Conclusion

In conclusion, HOF-on-MOF heterostructured material was successfully synthesized through the synergistic interactions of robust hydrogen bonds and π-π stacking forces. HOF-on-MOF exhibits highly peroxidase-like and laccase-like catalytic activity than Cu-MOF. Based on these characteristics, a bioprobe was developed for the colorimetric detection of β-BGT, facilitating the establishment of a highly sensitive detection strategy characterized by an exceptionally low limit of detection. The method was applied to measure β-BGT concentrations in human serum samples, achieving high recovery rates and reliable performance. This study offers a viable alternative to natural enzymes traditionally used in ELISA assays, presenting significant potential for snake venom detection. Furthermore, it broadens the application scope of framework materials, advancing their functional integration into biosensing and immunological diagnostics.

CRediT authorship contribution statement

Xiang Lai: Conceptualization, Investigation, Methodology, Software, Writing - original draft. **Xiaoqin Deng:** Visualization, Data Curation. **Tan Feng:** Visualization, Data curation, Writing - review & editing. **Lishen Yang:** Data curation. **Xingye Zheng:** Methodology. **Hang Chen:** Formal analysis. **Fengqi Zhou:** Data curation, Visualization, Data curation, Writing - review & editing. **Hongmin Zhu:** Software. **Jing Zeng:** Methodology, Conceptualization. **Wen-Hui Lee:** Resources. **Hui Zhao:** Conceptualization, Supervision, Project administration, Writing - review & editing, Resources. **Can-Peng Li:** Conceptualization, Supervision, Project administration, Writing - review & editing, Resources.

Declaration of Competing Interest

The authors declare that they have no known competing financial interests or personal relationships that could have appeared to influence the work reported in this paper.

Acknowledgments

This work was financially supported by Major Science and Technology Project of Yunnan Province (202302AE090022), Key Research and Development Program of Yunnan (202203AC100010), The National Natural Science Foundation of China (32160597, 32160236, 32371463), National Key Research and Development Program of China (2022YFC2601604), Cardiovascular Ultrasound Innovation Team of Yunnan Province (202305AS350021), Spring City Plan: the High-level Talent Promotion and Training Project of Kunming (2022SCP001), Yunnan University Graduate Student Research and Innovation Fund Program (KC-23234285).

Appendix A. Supporting information

Supplementary data associated with this article can be found in the online version at doi:10.1016/j.snb.2025.138510.

Data availability

Data will be made available on request.

References

[1] B.S. Naik, Dry bite" in venomous snakes: a review, Toxicon 133 (2017) 63–67.
[2] J.M. Gutiérrez, J.J. Calvete, A.G. Habib, R.A. Harrison, D.J. Williams, D.A. Warrell, Snakebite envenoming, Nat. Rev. Dis. Prim. 3 (2017) 17063.
[3] B. Mohapatra, D.A. Warrell, W. Suraweera, P. Bhatia, N. Dhingra, R.M. Jotkar, et al., Snakebite mortality in India: a nationally representative mortality survey, Plos. Negl. Trop. D. 5 (2011) e1018.
[4] R.A. Charvat, R.M. Strobel, M.A. Pasternak, S.M. Klass, J.L. Rheubert, Analysis of Snake venom composition and antimicrobial activity, Toxicon 150 (2018) 151–167.
[5] K. Amreen, M. Salve, S. Goel, Portable electrochemical platform with carbon fibre microelectrodes integrated on an OHP sheet for Snake venom analysis, IEEE Trans. NanoBiosci 22 (2023) 149–154.
[6] D. Morgenstern, G.F. King, The venom optimization hypothesis revisited, Toxicon 63 (2013) 120–128.
[7] Z.E. Selvanayagam, P. Gopalakrishnakone, Tests for detection of Snake venoms, toxins and venom antibodies: review on recent trends (1987-1997), Toxicon 37 (1999) 565–586.
[8] U. Puzari, A.K. Mukherjee, Recent developments in diagnostic tools and bioanalytical methods for analysis of Snake venom: a critical review, Anal. Chim. Acta 1137 (2020) 208–224.
[9] S. Shaheen, B. Fatima, D. Hussain, M. Imran, A. Najam, M. Najam-ul-Haq, Immobilization of antivenom polyvalent antibodies on MWCNTs@WO_3-Co_3O_5 capped with 3-mercaptopropionic acid for developing impedimetric immunosensor for Snake venom detection, Microchem. J. 209 (2025) 112797.
[10] J.F. Nong, Z. Huang, Z.Z. Huang, J. Yang, J.C. Li, F. Yang, et al., Development of sandwich ELISA and lateral flow assay for the detection of bungarus multicinctus venom, Plos Negl. Trop. D. 17 (2023) e0007014.
[11] L.P. Lee, C.H. Tan, S. Khomvilai, V. Sitprija, N. Chaiyabutr, K.Y. Tan, Characterizing and applying immunoglobulins in snakebite diagnostics: a simple and rapid venom detection assay for four medically important Snake species in Southeast Asia, Int. J. Biol. Macromol. 236 (2023) 123727.
[12] A. Waris, S. Hasnat, S. Hasan, S. Bano, A.O. Sultana, Ibhadon, et al., Development of nanozyme based sensors as diagnostic tools in clinic applications: a review, J. Mater. Chem. 11 (2023) 6762–6781.
[13] D.J. Wang, J. Wang, D. Liu, J.Y. He, M.Y. Wang, H.B. Huang, et al., Rapid and sensitive detection of Epstein-Barr virus antibodies in nasopharyngeal carcinoma by chemiluminescence strips based on iron-porphyrin single atom nanozyme, Nano. Res. (2023) 1827–1836.
[14] C. Wang, J. Gao, H. Tan, Integrated antibody with catalytic Metal–Organic framework for colorimetric immunoassay, Acs. Appl. Mater. Inter 10 (2018) 25113–25120.
[15] Z.Y. Lyu, S.C. Ding, N. Zhang, Y. Zhou, N. Cheng, M.Y. Wang, et al., Single-Atom nanozymes linked immunosorbent assay for sensitive detection of a beta 1-40: a biomarker of alzheimer's disease, Research 2020 (2020) 4724505.
[16] C.A. Halliwell, K. Jolley, K. Yendall, M.R.J. Elsegood, G.N. Parkinson, A. Fernandez, A simple and sequential strategy for the introduction of complexity and hierarchy in Hydrogen-Bonded organic framework (HOF) crystals for environmental applications, Angew. Chem. Int. Ed. 63 (2024) e202404452.
[17] G. Chen, L. Tong, S. Huang, S. Huang, F. Zhu, G. Ouyang, Hydrogen-bonded organic framework biomimetic entrapment allowing non-native biocatalytic activity in enzyme, Nat. Commun. 13 (2022) 4816.
[18] R.-B. Lin, B. Chen, Hydrogen-bonded organic frameworks: chemistry and functions, Chem 8 (2022) 2114–2135.
[19] W. Li, J. Shi, Y. Chen, X. Liu, X. Meng, Z. Guo, et al., Nano-sized mesoporous hydrogen-bonded organic frameworks for in situ enzyme immobilization, Chem. Eng. J. 468 (2023) 143609.
[20] V. Oskoei, M. Mathesh, W. Yang, Enhancing substrate channeling with Multi-Enzyme architectures in Hydrogen-Bonded organic frameworks, Chem. Eur. J. 30 (2024) e202401256.
[21] Y. Zhang, C. Zhang, W. Qian, F. Lei, Z. Chen, X. Wu, et al., Recent advances in MOF-based nanozymes: synthesis, activities, and bioapplications, Biosens. Bioelectron. 263 (2024) 116593.
[22] Z. Jiang, Y. Sun, Y. Rao, L. Yang, H. Xi, Q. Li, Isotopological entanglement of a metal–organic framework and a hydrogen-bonded organic framework for proton conduction, Nat. Synth. (2025) 1–10.
[23] J. Wang, Y. Mao, R. Zhang, Y. Zeng, C. Li, B. Zhang, et al., In situ assembly of Hydrogen-Bonded organic framework on Metal–Organic framework: an effective strategy for constructing Core–Shell hybrid photocatalyst, Adv. Sci. 9 (2022) 2204036.
[24] Y. Du, C. Ding, C. Deng, S. Banerjee, S. Agarwal, In situ constructed magnetic Core-Shell Hydrogen-Bonded organic Framework-on-Metal–Organic framework structure: an efficient catalyst for peroxymonosulfate activation, Adv. Funct. Mater. (2024) 2416686.
[25] H. Li, X. Liu, X. Feng, X. Guo, Z. Xu, Y. Wang, Rapid assessment of acetophenone using an anti-interfering triple-emission Ln^{3+}-functionalized HOF@MOF sensor, Talanta 280 (2024) 126718.

[26] Z. Zhang, B. Yan, Convolution neural Network-Assisted smart Fluorescent-Tongue based on lanthanide Ion-Induced forming MOF/HOF composite for differentiation of flavor compounds and wine identification, ACS Sens. 8 (2023) 3585–3594.
[27] S. Hu, H. Zhao, M. Liang, J. Hao, P. Xue, Interconversion and functional composites of metal–organic frameworks and hydrogen-bonded organic frameworks, Chem. Commun. 60 (2024) 8140–8152.
[28] S.-J. Yin, G.-C. Zheng, X. Yi, G.-P. Lv, F.-Q. Yang, A metal-organic framework@ hydrogen-bond framework as a matrix for MALDI-TOF-MS analysis of small molecules, Chem. Commun. 58 (2022) 6701–6704.
[29] X. Quan, B. Yan, A ternary dual-emission Eu(III)-functionalized HOF/COF hybrid: tryptophan, 5-hydroxyindoleacetic acid ratiometric fluorescence detection and latent fingerprint identification, Sens. Actuat. BChem. 409 (2024) 135590.
[30] W. Xu, Y. Wu, Y. Xu, X. Cai, W. Gu, C. Zhu, Metal–Organic Framework-Based artificial organelle corrects microenvironment interference for accurate intratumoral glucose analysis, Angew. Chem. Int. Ed. 62 (2023) e202308827.
[31] B.D. Howard, C.B. Gundersen Jr, Effects and mechanisms of polypeptide neurotoxins that act presynaptically, Annu. Rev. Pharm. 20 (1980) 307–336.
[32] B. Lin, J.-R. Zhang, H.-J. Lu, L. Zhao, J. Chen, H.-F. Zhang, et al., Immunoreactivity and neutralization study of Chinese bungarus multicinctus antivenin and lab-prepared anti-bungarotoxin antisera towards purified bungarotoxins and Snake venoms, Plos. Negl. Trop. D. 14 (2020) e0008873.
[33] J.-N. Zhu, X.-Q. Zhu, F.-F. Cheng, P. Li, F. Wang, Y.-W. Xiao, et al., Preparing copper doped carbon nitride from melamine templated crystalline copper chloride for Fenton-like catalysis, Appl. Catal. BEnviron. 256 (2019) 117830.
[34] S. Wang, W. Deng, L. Yang, et al., Copper-based metal–organic framework nanoparticles with peroxidase-like activity for sensitive colorimetric detection of staphylococcus aureus, Acs. Appl. Mater. Interfaces 9 (29) (2017) 24440–24445.
[35] Q. Yin, P. Zhao, R.J. Sa, G.C. Chen, J. Lu, T.F. Liu, et al., An Ultra-Robust and crystalline redeemable Hydrogen-Bonded organic framework for synergistic Chemo-Photodynamic therapy, Angew. Chem. Int. Ed. 57 (2018) 7691–7696.
[36] D. Manoj, R. Saravanan, J. Santhanalakshmi, S. Agarwal, V.K. Gupta, R. Boukherroub, Towards Green synthesis of monodisperse cu nanoparticles: an efficient and high sensitive electrochemical nitrite sensor, Sens. Actuat. BChem. 266 (2018) 873–882.
[37] S. Xu, H. Zhu, W. Cao, Z. Wen, J. Wang, C.P. François-Xavier, et al., Cu-Al_2O_3-g-C_3N_4 and Cu-Al_2O_3-C-dots with dual-reaction centres for simultaneous enhancement of Fenton-like catalytic activity and selective H_2O_2 conversion to hydroxyl radicals, Appl. Catal. BEnviron. 234 (2018) 223–233.
[38] L.Z. Gao, J. Zhuang, L. Nie, J.B. Zhang, Y. Zhang, N. Gu, et al., Intrinsic peroxidase-like activity of ferromagnetic nanoparticles, Nat. Nanotechnol. 2 (2007) 577–583.
[39] L. Gao, Q. Long, B. Cen, Q. Gao, M. Tan, L. Zhang, et al., Immobilization of a novel bacteriophage PpZDSS02 onto the peroxidase-mimicking Cu-MOF for colorimetric sensing of proteus penneri encompassing both promotion and inhibition mechanisms, Food Chem. 472 (2025) 142887.
[40] Y. Xu, J. Zhou, P. Sun, P. Li, D. Han, X. Wang, et al., The construction of peroxidase-like Cu-BDC@$FeMo_6$ for colorimetric detection of H_2O_2 and dopamine, Sep. Purif. Technol. 353 (2025) 128396.
[41] M.H. Ying, G.Z. Yang, Y.J. Xu, H.L. Ye, X. Lin, Y. Lu, et al., Copper fumarate with high-bifunctional nanozyme activities at different ph values for glucose and epinephrine colorimetric detection in human serum, Analyst 147 (2021) 40–47.
[42] R.G. Hadt, S.I. Gorelsky, E.I. Solomon, Anisotropic covalency contributions to superexchange pathways in type one copper active sites, J. Am. Chem. Soc. 136 (2014) 15034–15045.
[43] G. Ning, Q. Duan, H. Liang, H. Liu, M. Zhou, C. Chen, et al., One stone two birds: electrochemical and colorimetric dual-mode biosensor based on copper peroxide/ covalent organic framework nanocomposite for ultrasensentive norovirus detection, Food Sci. Hum. Well 13 (2024) 920–931.
[44] X. Liu, P. An, Y. Han, H. Meng, X. Zhang, MOF-818(Cu)-derived bi-nanozymes of laccase and catecholase mimics and colorimetric sensing to epinephrine, Microchem. J. 201 (2024) 110559.
[45] J. Wang, R. Huang, W. Qi, R. Su, B.P. Binks, Z. He, Construction of a bioinspired laccase-mimicking nanozyme for the degradation and detection of phenolic pollutants, Appl. Catal. BEnviron. 254 (2019) 452–462.
[46] M. Li, Y. Xie, L. Lei, H. Huang, Y. Li, Colorimetric logic gate for protamine and trypsin based on the Bpy-Cu nanozyme with laccase-like activity, Sens. Actuat. BChem. 357 (2022) 131429.
[47] P. Dong, K. Gao, L. Zhang, et al., Hydrogen bond-assisted construction of MOF/ semiconductor heterojunction photocatalysts for highly efficient electron transfer, Appl. Catal. BEnviron. Energy 357 (2024) 124297.
[48] E.G. Rowan, What does β-bungarotoxin do at the neuromuscular junction? Toxicon 39 (2001) 107–118.

Xiang Lai is currently pursuing his PhD at Yunnan University in Kunming, China. His main research focus is on framework material-based biosensors.

Xiaoqin Deng is currently pursuing his master's degree at Yunnan University, Kunming, China. Her research interests are mainly focused on biosensors for biomarker. Her research interests are focused on the study of inflammation in nanomaterials.

Tan Feng is currently pursuing her master's degree at Yunnan University, Kunming, China. Her research interests are mainly focused on biosensors for biomarkers. Her research interests are focused on the study of inflammation in nanomaterials.

Lishen Yang is currently pursuing her master's degree at Yunnan University, Kunming, China. Her research interests are focused on the study of inflammation in nanomaterials.

Xingye Zheng is currently pursuing her master's degree at Yunnan University, Kunming, China. Her research interests focus on anti-tumor studies based on framework materials.

Hang Chen is currently pursuing his master's degree at Yunnan University, Kunming, China. His research interests are focused on the study of inflammation in nanomaterials

Fengqi Zhou is currently pursuing his master's degree at Yunnan University, Kunming, China. His research interests focus on anti-tumor studies based on carbon quantum dots.

Hongmin Zhu is currently pursuing her master's degree at Yunnan University, Kunming, China. Her research interests focus on building functional biomaterials and nanodelivery systems.

Jing Zeng received his master's degree from Yunnan University, Kunming, China. His research interests focus on biosensors based on organic framework materials.

Wen-Hui Lee is an associate researcher at Kunming Institute of Zoology, Chinese Academy of Sciences. His research interests focus on the molecular biodiversity, structure and function of amphibian reptile toxin proteins and peptides.

Hui Zhao is a professor in Yunnan University, Kunming, China. Her current research interests are biosensor and functional genes.

Can-Peng Li is a professor in Yunnan University, Kunming, China. His research interests are focused on fluorescence/electrochemical sensors, biosensors, and functional food.